Polarized near-edge x-ray-absorption fine structure spectroscopy of C 60 - functionalized 11-amino-1-undecane thiol self-assembled monolayer: Molecular orientation and Evidence for C 60 aggregation

Archita Patnaik, Koji K. Okudaira, Satoshi Kera, Hiroyuki Setoyama, Kazuhiko Mase, and Nobuo Ueno

Citation: The Journal of Chemical Physics **122**, 154703 (2005); doi: 10.1063/1.1880952
View online: http://dx.doi.org/10.1063/1.1880952
View Table of Contents: http://scitation.aip.org/content/aip/journal/jcp/122/15?ver=pdfcov
Published by the AIP Publishing

Polarized near-edge x-ray-absorption fine structure spectroscopy of C_{60}-functionalized 11-amino-1-undecane thiol self-assembled monolayer: Molecular orientation and Evidence for C_{60} aggregation

Archita Patnaik[a)]
Department of Chemistry, Indian Institute of Technology Madras, Chennai-600036, India

Koji K. Okudaira, Satoshi Kera, and Hiroyuki Setoyama
Department of Materials Technology, Chiba University, Yayoi-cho, Inageku, Chiba 2638522, Japan

Kazuhiko Mase
Institute of Materials Structure Science, Tsukuba 305-0801, Japan

Nobuo Ueno
Department of Materials Technology, Chiba University, Yayoi-cho, Inageku, Chiba 2638522, Japan

(Received 25 October 2004; accepted 3 February 2005; published online 18 April 2005)

Near-edge x-ray-absorption fine structure (NEXAFS) spectroscopy was adopted to probe the unoccupied electronic states of C_{60} anchored onto an organized assembly of 11-amino-1-undecane thiol on Au(111). The polarization dependence of the intensity of π^* resonance associated with C_{60} π network revealed the self-assembled monolayer (SAM) system to be oriented with an average molecular tilt angle of 57° with respect to the surface normal. Invoking the absence of solid-state band dispersion effects and in comparison to solid C_{60} and /or 1-ML C_{60}/Au(111), the electronic structure of the resulting assembly was found dominated by spectral position shift and linewidth and intensity changes of the lowest unoccupied molecular orbital (LUMO), LUMO+1, and LUMO +2 orbitals. The latter implied hybridization between N P_z of $-NH_2$ group of thiolate SAM and π levels of C_{60}, resulting in a nucleophilic addition with a change in the symmetry of C_{60} from I_h to $C1$ in the SAM. Occurrence of a new feature at 285.3 eV in the NEXAFS spectrum, assigned previously to π^* graphitic LUMO, signified the formation of aggregated clusters, $(C_{60})_n$ of C_{60} monomer. Low tunneling current scanning tunneling microscopy confirmed them to be spherical and stable aggregates with $n \sim 5$. © *2005 American Institute of Physics*. [DOI: 10.1063/1.1880952]

I. INTRODUCTION

The electronic structure of C_{60} is characterized by the delocalized and highly degenerate orbitals due to π bonding and I_h symmetry,[1,2] and the intermolecular bonding is governed by van der Waals interactions.[3] Use of different experimental methods such as photoelectron spectroscopy,[4–6] inverse photoemission,[7] and x-ray absorption spectroscopy[8,9] have given extensive experimental data on the electronic structure of C_{60}. Terminello *et al.*[9] investigated the x-ray-absorption fine structure of solid C_{60} in terms of sharp π^* transitions at low energy and at higher energies; broader resonances were attributed to σ^*-like orbitals. Based on the observed energy splittings of the π^* resonances and the narrow linewidths, C_{60} films were explained to resemble a molecular solid with strong intramolecular rather than intermolecular interactions. Direct *in situ* comparison of C 1*s* absorption spectra of C_{60} in gas and solid phases[10] revealed solid-state interactions to play a minor role in this material and that the electron correlation effects were predominantly intramolecular. Occupied and unoccupied electronic states of C_{60}/Au(110) were studied by Maxwell *et al.*[11] Hybridization between the C_{60} lowest unoccupied molecular orbital (LUMO) and the occupied states around the substrate Fermi level in the core excited final state was observed. Further, a comparison of the near-edge x-ray-absorption fine structure (NEXAFS) spectra for a 1-ML sample compared with a thick film indicated hybridization to occur with the unoccupied states, leading to the LUMO+1 feature at 285.8 eV. Brueh-wiler *et al.*[12] presented C 1*s* autoionization (C 1*s* $\rightarrow$LUMO) of Xe matrix-isolated C_{60} molecules, showing LUMO levels beginning at 284.5 ± 0.05 eV and were ascribed as core-hole perturbed levels derived from the $5t_{1u}$ (LUMO), $2t_{1g}/5t_{2u}$, and $8h_g$ orbitals of C_{60}.

The structural uniqueness and chemical identity of C_{60} have rendered numerous applicabilities of the material. Attachment of fullerene moieties to the tail groups of self-assembled monolayers (SAMs) provides a novel opportunity. Chemical bonding of C_{60} to the surfaces of SAMs not only provides discrete monolayers of C_{60} but also organized assemblies where C_{60} moieties will remain immobilized on the surface.[13–16] The specific interaction of Au with S and other soft nucleophiles and its low reactivity towards most hard acids and bases make it possible to vary the structure of the terminal group, permitting a wide range of functional groups onto a surface.

Focusing on the *in situ* preparation of a C_{60}-terminated thiol SAM, the present work involves initiating a reaction

[a)]Electronic mail: archita59@yahoo.com

between C_{60} and the terminal $-NH_2$ group of an already formed 11-amino-l-undecane thiol (11-AUT) SAM on Au(111) surface, taken as a supporting matrix. In contrast to neat C_{60} films, the orientation in C_{60}-terminated SAM may vary due to structural/conformational relaxation of the surrounding thiol molecules in the voids created by the large diameter of C_{60}. The purpose of this investigation is to unravel the molecular orientation and electronic structure (unoccupied molecular orbitals) of the C_{60}-terminated 11-AUT SAM adopting NEXAFS spectroscopy and scanning tunneling microscopy (STM).

NEXAFS spectroscopy allows us to study local unoccupied states of a system by measuring absorption close to a core-level ionization threshold. Self-assembly of amphiphilic molecules, alkane thiols, and carboxylic acids on Au and Indium tin oxide (ITO) surfaces has been investigated by NEXAFS spectroscopy in determining molecular orientation and intermediate steps in self-assembly.[17–19] For the C_{60}-functionalized 11-AUT SAM, excitation of the C 1*s* electrons to the unoccupied C_{60} π^* manifold, to the molecular Rydberg states associated with $(C–H)^*$ resonance of the alkyl chain, and for both cases to σ^* states along the (C–C) sigma bond and over the cage is envisaged. Here the excited electron populates the molecular orbitals whose degeneracy has been broken by the symmetry reducing effect of the core hole.[11,20] The strongest peaks in the spectrum thus would correspond to excitations to energy levels localized by the core hole, similar to core excitons in large systems.[12] For systems with unsaturated C═C bonds, as in C_{60}, the lowest-energy excitations will occur to the π^* state, with energies less than the 1*s* ionization potential.[9]

By virtue of its rigid well-defined geometry in solution phase, C_{60} molecule is exempted from subtle conformational or solvent-dependent intramolecular vibrational changes and displays a trend towards aggregate/cluster formation.[21–25] A thermodynamic approach to the description of cluster formation in C_{60} solutions was put forward.[26] The above phenomenon thus paves way for investigating the unoccupied electronic states of the possible C_{60}-aggregated phase, formed during self-assembly of C_{60}-anchored 11-AUT from benzene solution.

II. EXPERIMENTAL SECTION

A. Materials

11-Amino-1-undecane thiol hydrochloride $[HS–(CH_2)_{11}–NH_3^+Cl^-]$ was purchased from Dojindo Laboratories, Japan. C_{60} of 99.95% purity was used without any further purification. Ethanol (AR grade) and toluene (AR grade) were purchased from Aldrich Chemicals Co. and used as received. The absence of characteristic NH_3^+ vibrations in the Fourier transform infrared spectrum at 3100 cm^{-1} indicated the terminal group of the SAM to be in its free $-NH_2$ state and not in the protonated form[27] where the ions are believed to have been washed away during the posttreatment rinsing.

B. Vacuum deposition of Au(111) on mica

For this purpose, freshly cleaved 4×4 cm^2 mica strips were preannealed by resistive heating at 300 °C for 8 h in order to enhance the formation of large Au(111) terraces. Keeping the mica substrate's temperature at ~150 °C, gold evaporation was carried out at 10^{-8} Torr pressure and with a deposition rate of ~0.3 nm/s. The Thickness of the Au layer was estimated to be ~200 nm. X-ray diffraction analysis indicated Au(111) single-crystal formation.

FIG. 1. The molecular conformation and the energy-minimized structure of C_{60}-anchored 11-AUT SAM, estimated with density-functional theory at level Becke 3 Lee–Yang–Parr (B3LYP) and basis set Los Alamos National Laboratory double zeta (LANL2DZ). The estimated length of the molecule is shown with S atom bonded to the threefold hollow site of gold hexagonal lattice, forming an arrangement of $(\sqrt{3}\times\sqrt{3})$ $R30°$ overlayer structure. Au and H atoms are shown in deep gray, N and S in black, and C atoms in light gray.

C. Monolayer preparation

Self-assembled monolayers of 11-AUT were prepared by immediately soaking the annealed (200 °C for 3 h) gold-coated mica strips in ~1-mM 11-AUT ethanol solution at room temperature for 24 h. The aminothiolate SAMs thus formed were exhaustively cleaned with ethanol to get rid of the physisorbed moieties and were immediately dipped further in a freshly prepared ~1-mM C_{60} solution in benzene and kept for 24 h. The SAMs thus formed were washed with benzene, ethanol, and dichloromethane and used for respective experimental investigations after drying in air. Figure 1 illustrates the energy-optimized structure of the C_{60}-functionalized 11-AUT SAM.

D. NEXAFS spectroscopy

NEXAFS measurements were performed at the beamline BL13C of the photon factory at National Laboratory for High Energy Physics (KEK-PF) at Tsukuba. The absorption spectra were obtained in the total electron yield mode at a pressure of 2×10^{-10} Torr. The photon energy calibration was performed with π^* (C═O) feature of purified polymethylmethacrylate (PMMA) at 288.7 eV and the energy resolution was estimated to vary between 0.5 and 0.6 eV at the C *K* edge.

K-shell resonance's angular dependence is studied with highly directional bonds and molecular orbitals of molecules, chemisorbed on surfaces whose symmetries are different from that of the free molecule. The spectroscopy, being a localized one, probes the amplitude and directionality of the upper-state molecular orbitals on the excited atom. Further, the electronic transitions from C 1*s* into the unoccupied molecular orbitals obey dipole selection rules and show strong dependence on the polarization of incident photons. The in-

tensity variations as a function of photon incidence angle are thus used in our experiments to determine the average molecular orientation of the SAMs on Au(111) surface. The spatial orientation of the π^* and σ^* orbitals will be represented as a vector type.

E. STM imaging

Series of STM images of 11-AUT and C_{60}-functionalized 11-AUT were acquired with Digital Instruments Nanoscope III in air with the samples placed in an antivibration chamber. Images were acquired at a constant current mode with a low tunneling current at 0.2 nA. The sample bias voltage with respect to the Pt/Ir tip was set between 300 and 500 mV and the tunneling current set point varied between 10 and 100 pA.

III. RESULTS AND DISCUSSION

A. NEXAFS spectroscopy

1. C K-edge NEXAFS peak assignment

Figure 2(a) shows the C *K*-edge NEXAFS spectra of the C_{60}-functionalized 11-AUT recorded for photon incidence angle, α with respect to the surface normal, varying from 0° to 70° (grazing incidence). Normalization to the incident photon flux was carried out by dividing the raw NEXAFS spectra (I_s) by the monochromator transmission function determined on a sputter-cleaned Au sample (I_0). The spectra in Fig. 2(a) show the most prominent resonances at 284.9 (A) and 286.6 eV (B) of the π^* LUMO and LUMO+2 of C_{60} and at 288.8- (C) and 293.3- eV (D) features, attributed to R^* and σ^*(C–C), σ^*(C–N) resonances of the $-NH_2$-substituted alkyl chain, respectively. In Fig. 2(b), a distinct angle dependence of the most prominent π^* feature in the normalized spectra indicates the presence of a well-ordered monolayer structure. For comparison, Fig. 2(c) depicts the angular variation in the aminothiol (11-AUT) SAM. Prominent absorptions are observed at 288.8 and 292.9 eV and are attributed to R^* and σ^*(C–C) resonances. In Figs. 2(a) and 2(b), the π^* transitions are sharp at 284.9 eV and the onset transitions to σ^* states are associated with a steplike increase in absorption. Resonance peaks from C 1*s* core level to the unoccupied molecular orbitals of C_{60} molecule in 0.25-ML (monolayer) and 5-ML C_{60} on Si (111) were reported at 284.9 (LUMO), 286.1 (LUMO+1), 286.7 (LUMO+2), 288.7 (LUMO+3), 291.3, 292.3, and 293.3 eV; the first four features below the ionization potential of 289.6 eV were attributed to π^* resonances and the rest to σ^* transitions,[28] respectively, arising as a result of transition of the C 1*s* electron into the molecular Rydberg and σ^* states associated with the hydrocarbon backbone.[29] The present R^* feature at 288.7 eV is shifted ~1 eV to the higher photon energy with respect to $-CH_3$-terminated thiol SAMs,[30–32] implying a possible influence of the $-NH_2$ end group on the alkanethiol backbone. The energies of C–C and C–N bond prepared localized components are nearly degenerate, making it difficult to distinguish the individual orbital contributions in the C *K*-edge absorption features. Further, contribution from the latter is low owing to a much smaller stoichiometry in the mono-

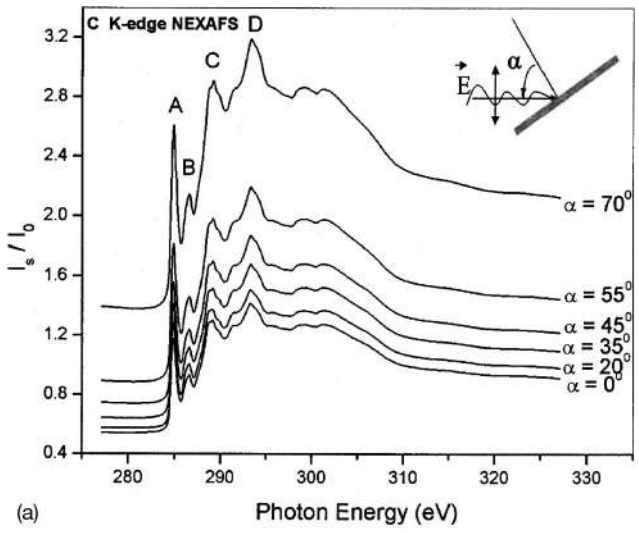

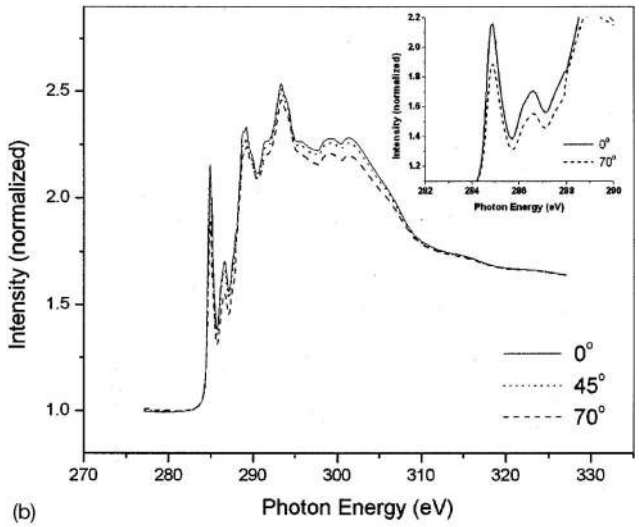

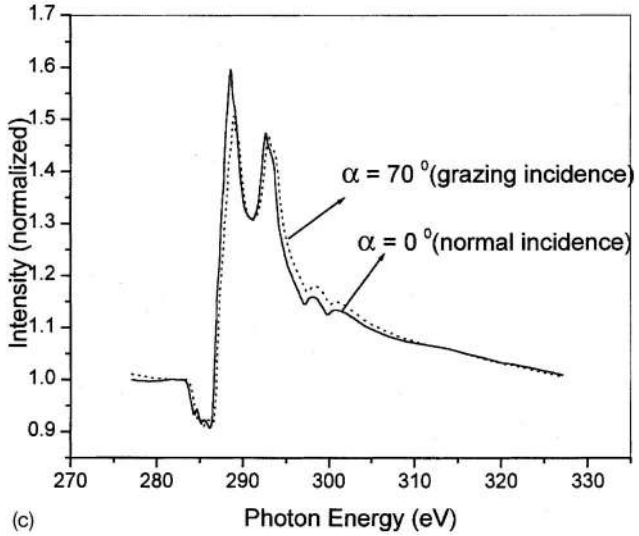

FIG. 2. (a). C *K*-edge NEXAFS spectra of C_{60}-functionalized 11-AUT SAM recorded for photon incidence angle (α) varying between 0° and 70°. The inset defines α from the surface normal along with the electric vector $\vec{E}$ of the photon beam. (b) Normalized C *K*-edge NEXAFS spectra of C_{60}-functionalized 11-AUT SAM for photon incidence angles α=0°, 45°, and 70°. The inset shows an expanded version, depicting the angular intensity variation of the π^* resonance. (c). Normalized C *K*-edge NEXAFS spectra of 11-AUT SAM for photon incidence angles α=0° and 70°.

layer. Similar observations were noticed with the C *K*-edge absorption characteristics of an ordered monolayer growth of glycene adsorbed on Cu (110),[33] where chemisorption involving two functional groups on Cu (110) was envisaged.

In Fig. 2(c), a partial dichroism is observed with the R^* and σ^*(C–C) resonances for the 11-AUT SAM; such an effect could be attributed to the presence of a molecular dipole layer from a polar end group such as the $-NH_2$ group that shifts the surface potential with respect to pristine Au(111) electrode.[34] The C_{60}-functionalized 11-AUT SAM does not reveal dichroism in the R^* and σ^*(C–C) resonances in Fig. 2(b), even though distinct changes in the π^* resonance intensities for 0° and 70° are observed along with small σ^* intensity variations as a function of angle of incidence. In the case of the C_{60}-functionalized 11-AUT SAM, the exact orientation of the π^* orbital cannot be visualized. However, as shown in Fig. 2(b), the reduced π^* intensity at grazing incidence implies the C_{60} molecules not to remain in a flat-lie orientation.

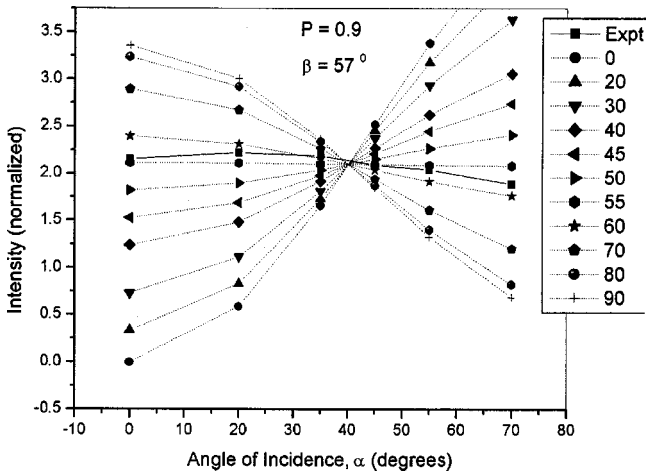

FIG. 3. Graphical representation of normalized NEXAFS intensities of C_{60}-functionalized 11-AUT SAM as a function of angle of incidence of photons, according to Eq. (3). The filled squares connected with a solid line are experimental points.

2. The angular dependence of NEXAFS resonance intensities and the molecular orientation

The direction of maximum orbital amplitude determines the angular dependence of *K*-shell spectra. For vector-type orbitals, the absolute angle-integrated intensity I_v is given as[20]

$$I_\nu = A[PI_v^{\mathrm{II}} + (1-P)I_v^{\perp}], \tag{1}$$

where A is a constant and P is the degree of photon polarization, taken as 0.9 in our experiments. The $I_v^{\parallel}$ and $I_v^{\perp}$ represent resonance intensities of the vector orbitals for the parallel and perpendicular components of the electric-field vector. The transition intensity depends on the orientation of the electric-field vector (parallel and perpendicular) components relative to molecular orientation. The dominant component is the parallel one, tilted at angle θ to the surface normal, where $\theta=(90-\alpha)$ in the present investigation. We define the photon incidence angle as α with β as the molecular tilt angle with respect to the surface normal. ϕ is the azimuthal orientation of the molecule with respect to the substrate. Equation (1) is thus further written as

$$I_v = A\begin{bmatrix} P(\cos^2\theta\cos^2\beta + \sin^2\theta\sin^2\beta\cos^2\phi \\ +2\sin\beta\cos\beta\sin\theta\cos\theta\cos\phi) \\ +(1-P)\sin^2\beta\sin^2\phi \end{bmatrix}. \tag{2}$$

For higher substrate symmetry, Eq. (2) reduces to

$$I_\nu = A\left[\tfrac{1}{3}P\left\{1+\tfrac{1}{2}(3\cos\theta-1)(3\cos^2\beta-1)\right\}+(1-P)\times\left(\tfrac{1}{2}\sin^2\beta\right)\right] = A\left[\tfrac{1}{3}P\left\{1+\tfrac{1}{2}\left[3\cos^2(90-\alpha)-1\right]\times(3\cos^2\beta-1)\right\}+(1-P)\left(\tfrac{1}{2}\sin^2\beta\right)\right]. \tag{3}$$

Using the above equation and the normalized intensity for the π^* LUMO of C_{60}, we estimated the average molecular orientation, "β" of the C_{60}-functionalized 11-AUT SAM as 57° with $A=6.3$, as shown in Fig. 3. For the 11-AUT SAM, the normalized intensities of R^* resonance around the C–H bond direction were taken and adopting the above procedure, the molecular tilt angle with respect to the surface normal was estimated to be 56°. The experimental intensities show small but clear α dependence. While addressing molecular order at the outer surface of the monolayer on gold, this observation of similar molecular tilt angles in both SAMs implies that the molecular orientation in the C_{60}-functionalized 11-AUT SAM is not end group dominated. This has strong evidence from the low intensities observed in the ultraviolet photoelectron spectra[35] resulting from an all-trans alkyl chain with the C_{60} moieties highly tilted from the surface normal. Further, thiophene-terminated monolayers have been found to satisfy the above observation. It is to be mentioned here that along with the constituent atoms of the end group, their spatial positions also play an important role in controlling the molecular orientation in space. In 11-AUT SAM, the $-NH_2$ group being polar, its secondary coordination with Au surface via the unprotonated N heteroatom[36,37] freezes the rotational degrees of freedom of the alkyl chain resulting in a discrete molecular tilt angle of 56°. Weak bond formation between the lone pairs of electrons on the $-NH_2$ group and the Au(110) surface has been reported both theoretically and experimentally, attributing structural stability to LL cysteine dimer.[38] The N–Au interaction energy was calculated to be 0.2 eV with a N–Au distance of 2.4 A° in the LL dimer and 2.7 A° in the DL dimer. A larger N–Au distance in the latter resulted in lesser stability to the adsorbate by 0.5 eV. In the present work, the alkane chain length being long, we do not anticipate any bonding between $-H_2N$ and Au(111). However, a large molecular tilt angle of 56° from the surface normal does imply an existing interaction between them.

A large molecular tilt angle in the present investigtaion was further thought of from the context of a reported x-ray incidence angle of 54.7°, the magic angle, where the measured intensity distribution becomes independent of molecular orientation for a perfect linear polarization, $P=1$.[20] However, in the present sets of experiments, $P\approx 0.9$ and accordingly, the magic angle of incidence according to Stoehr, given as

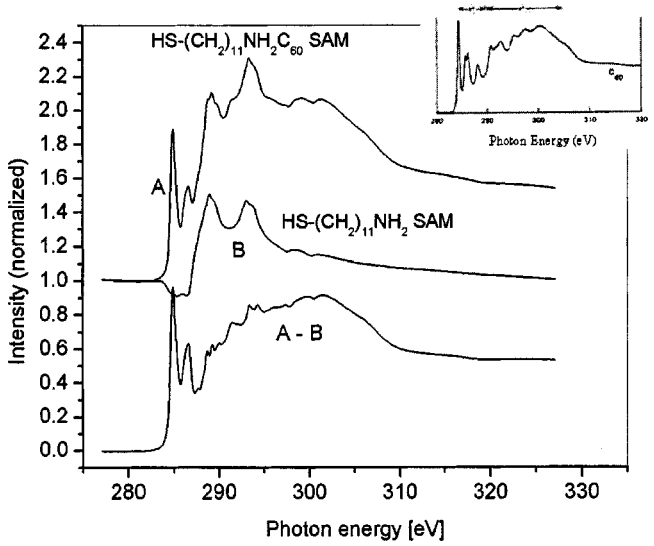

FIG. 4. Comparative NEXAFS spectra shown for 11-AUT SAM on Au(111)→B and the corresponding C_{60}-functionalized 11-AUT on Au(111)→A. The difference spectrum (A-B) resembles the NEXAFS spectrum of solid C_{60}, shown in the inset, *vide* Ref. 9.

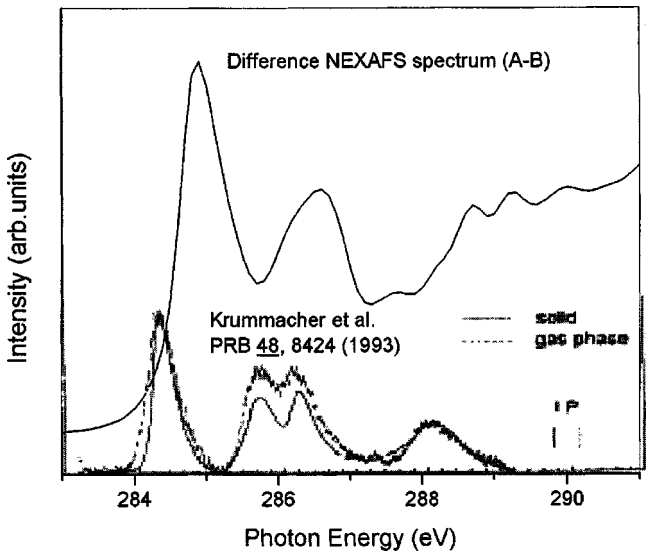

FIG. 5. A comparison between the C 1*s* near-edge absorption spectrum of (A-B) in Fig. 4 with that of solid and gas phase spectra of C_{60} (*vide* Ref. 10). The vertical bars at 290.1 and 289.75 eV indicate C 1*s* ionization potentials relative to vacuum level for the respective phases.

$$\theta = \sin^{-1}\sqrt{\left(1-\frac{1}{3P}\right)},$$

turns out to be 52.5°, which is much lower than the observed value of 57°, thus validating the latter.

3. Evidence for C_{60} aggregation and its bonding with $-NH_2$ group of the 11-AUT SAM

Figure 4 illustrates the C *K*-edge NEXAFS spectra of the C_{60}-functionalized 11-AUT SAM (A), the 11-AUT SAM (B), and the difference between them as (A-B). For a comparison, in the inset, the NEXAFS spectrum of solid C_{60} reported by Terminello *et al.*[9] is shown. The difference spectrum (A-B) closely resembles the solid-state spectral features of solid C_{60}.

In Fig. 5, from an expanded (A-B) spectrum in the photon energy region of 283–291 eV, evidence for peak position shifts, linewidth broadening, and intensity reduction for the LUMO features is revealed, when compared with the solid/gas phase NEXAFS spectra of C_{60}.[10] LUMO+1 and LUMO+2 are not resolved in the former on account of the instrumental resolution varying between 0.5 and 0.6 eV. The noticeable linewidth broadening of LUMO, LUMO+1, and LUMO+2 features in the gas phase spectrum has been ascribed to the population of excited vibronic states in the C_{60} beam prior to excitation. In the deconvoluted lower-energy region of the NEXAFS spectrum of the C_{60}-functionalized 11-AUT SAM in Fig. 6, we notice that the dominating LUMO at 284.9 eV is accompanied by a new feature at 285.3 eV, with a relative intensity of 22% in reference to the LUMO. We attribute this feature to π^* LUMO of the C_{60}-aggregated phase, $(C_{60})_n$, complying with the reported π^* peak of graphite at 285.35 eV.[9] The electron-diffraction pattern of C_{60} aggregates and C_{60} fullerites grown from millimolar benzene solution[39–43] was found to be highly oriented with discrete diffraction spots. Their structure analysis resembled a graphitelike hexagonal-close-packing (hcp) lattice structure which justifies the above attribution. A further confirmation to aggregation was obtained from STM imaging, where a two-dimensional (2D) profile of these aggregates in the next section will be highlighted.

The sharp π^* resonances of C_{60} were explained as a characteristic of molecular orbital-like final states[20,44] implying C_{60} in the condensed state/films to contain discrete, chemically noninteractive molecules.[45] However, intermolecular effects[12] were apparent in the C 1*s* absorption spectra of solid C_{60} as compared to the Xe-matrix isolated one; a greater broadening was found for the thick-film spectrum, in particular, the LUMO+1 and LUMO+2 features in the solid were noticeably broader than in the molecule and were independent of temperature for the thick film in the range $30 < T < 300$ K. The Gaussian deconvolution yielded widths ~0.25 eV for LUMO+1 and LUMO+2 peaks. A compara-

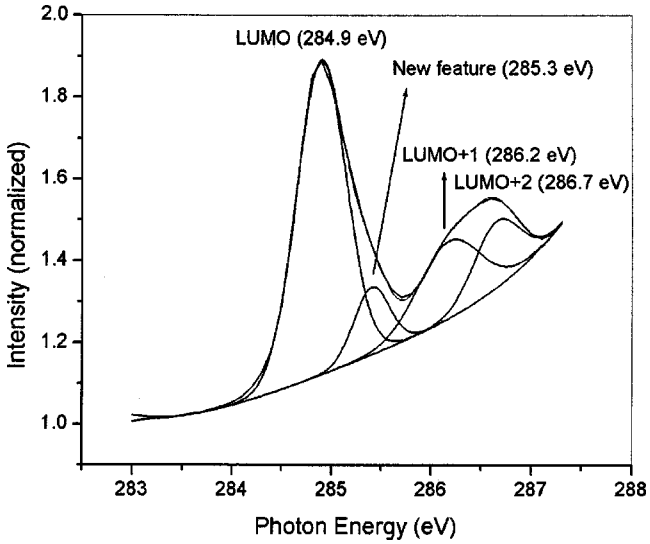

FIG. 6. Gaussian peak fitting of the lower-energy region of the NEXAFS spectrum of C_{60}-functionalized 11-AUT illustrating the new $(C_{60})_n$ π^* feature.

TABLE I. Experimental energies, assignments, and line-shape analysis for the C *K*-edge NEXAFS spectra of C_{60}-functionalized 11-AUT SAM and their comparison with literature. The values inside the bracket are for the difference spectrum (A-B) in Fig. 4. The higher width and relative intensity for the LUMO+1 and the new feature for (A-B) as compared to "A" could be from absorption by slightly contaminated Au photodiode as seen in the preedge region of spectrum B.

	This work				C_{60} (solid) (Ref. 10)		
Feature	LUMO	LUMO+1	LUMO+2	New feature	LUMO	LUMO+1	LUMO+2
Photon energy (eV)	284.9 (284.9)	286.2 (286.2)	286.7 (286.7)	285.3 (285.3)	284.3	285.7	286.2
Polarization dependence/assignment	π π^*cage	π π^*cage	π π^*cage	π π^* $(C_{60})_n$	π π^*cage	π π^*cage	π π^*cage
Gaussian width (eV)	0.58 (0.56)	0.73 (0.87)	0.54 (0.54)	0.42 (0.54)	0.3	0.50	0.40
Relative intensity	1.0 (1.0)	0.25 (0.40)	0.21 (0.27)	0.22 (0.33)	1.0	0.45	0.47

tive investigation on the π^* LUMOs of C_{60} and graphite[9] showed the lowest LUMO peak shifted from 284.3 eV for the former to 285.35 eV for the latter, with a large increase in the peak width for the latter. For solids with infinite periodicity as in graphite, the π orbitals interact to form bands. The NEXAFS resonances thus correspond to transitions to flat-bands having high density, when averaged over the Brillouin zone. However, we do not observe such a remarkable width change between the 284.9- and 285.3-eV features in Fig. 6. Table I lists a comparative account of NEXAFS spectral peak positions, widths, and the relative intensities (with respect to LUMO) for the C_{60}-functionalized 11-AUT SAM, the difference spectrum, and for solid C_{60}, *vide* Ref. 10.

We focus on the C_{60}-functionalized 11-AUT SAM spectral features for discussion. The LUMO peak position has shifted from 284.3 eV in the solid C_{60} to 284.9 eV in the SAM, as a result of covalent $-NH_2$ addition to the C_{60} cage. The C 1*s* NEXAFS peaks corresponding to unoccupied molecular orbitals for 1-ML C_{60}/Au(111) were observed at 284.5 (LUMO), 285.9 (LUMO+1), 286.5 (LUMO+2), and 288.3 eV(LUMO+3).[46] It is worth mentioning here that the present LUMO position at 284.9 eV, which is different from the NEXAFS feature of solid C_{60} at 284.3 eV, has also been described as the characteristic chemisorbed state for C_{60} monolayer film adsorbed on Si (111)-(7×7) (Ref. 47) and Si (001)-(2×1) surfaces.[28] Whereas for ionic bonding of C_{60} on Cu(111), LUMO shifted to lower photon energy with decreased intensity, attributed to charge transfer from the substrate to C_{60} in the NEXAFS spectra,[48] on Al(111), C_{60} bound covalently. A higher photon energy shift was observed without a change in LUMO intensity, but with a decrease in LUMO+1 intensity.[49] Fluorination of C_{60} resulted in a decrease of intensity as well as width of the π^* band region at the expense of an enhancement in the intensity of σ^* features.[50] In the present experiments, the LUMO is also broadened by 0.28 eV with respect to a peak width of 0.3 eV for the 284.3-eV LUMO feature for the solid phase of C_{60}.[10] Further, the observed LUMO width of 0.58 eV is similar to the theoretical dispersion of 0.5 eV for solid C_{60}, calculated by Saito and Oshiyama.[51] Thus we conclude that solid-state band dispersion in terms of peak broadening and/or shifts does not play a major role in these spectra.

$-NH_2$ group addition to C_{60} is a nucleophilic addition reaction at one of the 6:6 double bonds of the carbon cage.[52] A symmetry change from I_h to $C1$ for C_{60}-functionalized 11-AUT SAM on Au(111) surface was calculated by us with ground-state density-functional theory (DFT) calculations. Although LUMO peak width enhancement by 0.28 eV implies bonding interaction to be sufficient to dominate the linewidth, direct evidence of hybridization between N P_z and C_{60} π levels does not seem inevitable and is in compliance with the fact that NEXAFS linewidths are not dominated by hybridization in the core-excited final state.[11] Thus, we obtained further experimental evidence for the asymmetric $-NH_2$ addition to C_{60} from the associated linewidths and intensities with the LUMO+1 and LUMO+2 molecular orbitals by extending the energy region beyond LUMO. The LUMO+1 state in the figure at 286.2 eV is one of the triply degenerate LUMOs of C_{60} having the largest spatial extent due to larger overlap with neighboring molecules[12,53,54] and has attenuated substantially, as seen in Table I, from a relative intensity of 0.45 in solid phase to 0.25 in the self-assembled monolayer. Further, an observable linewidth broadening from 0.5 to 0.73 eV for this feature is also noted. The resulting linewidth and intensity variations on account of symmetry reduction and chemical shifts thus imply the LUMO+1 to take part in bonding, where the electron deficient C_{60} undergoes nucleophillic addition with the $-NH_2$ group. The increase in full width at half maximum (FWHM) of LUMO+1 and LUMO+2 implies removal of degeneracy of the molecular orbitals and hence a change in the bonding state of carbon from sp^2- to sp^3-hybridized state results. Nonetheless, the survival of the LUMO+1 and LUMO+2 peaks in the NEXAFS spectrum indicates that the conduction band is only slightly disturbed. LUMO+3 was not taken into account in the discussion because of its convolution with the NEXAFS features of 11-AUT SAM at ~288 eV, attributed to $(C-H)^*$ resonances. A qualitative picture of the LUMOs of C_{60}-functionalized 11-AUT in Fig. 7(a) and pristine C_{60} in Fig. 7(b) is presented, evidencing a drastic change in the electron-density distribution in the corresponding LUMOs as a result of symmetry change from I_h, in pristine C_{60} to $C1$ in the C_{60}-functionalized 11-AUT SAM. It must also be mentioned that the threefold degeneracy of the LUMOs in pris-

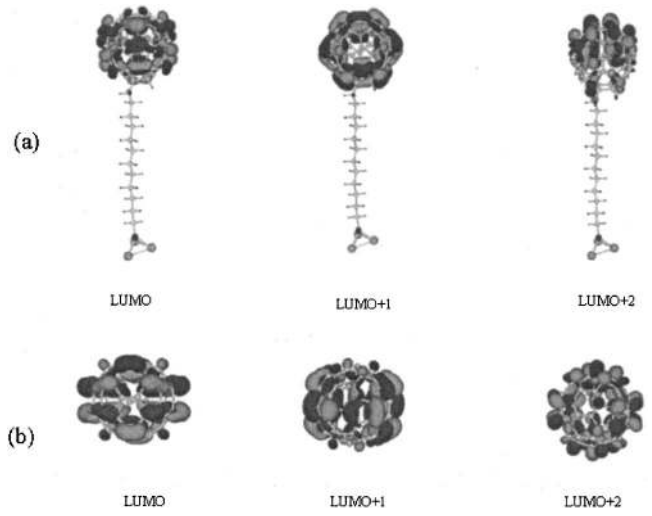

FIG. 7. Typical lowest unoccupied molecular orbitals of (a) C_{60}-functionalized 11-AUT, and (b) solid C_{60}, calculated from DFT with linear combination of atomic orbitals (LCAO) approach.

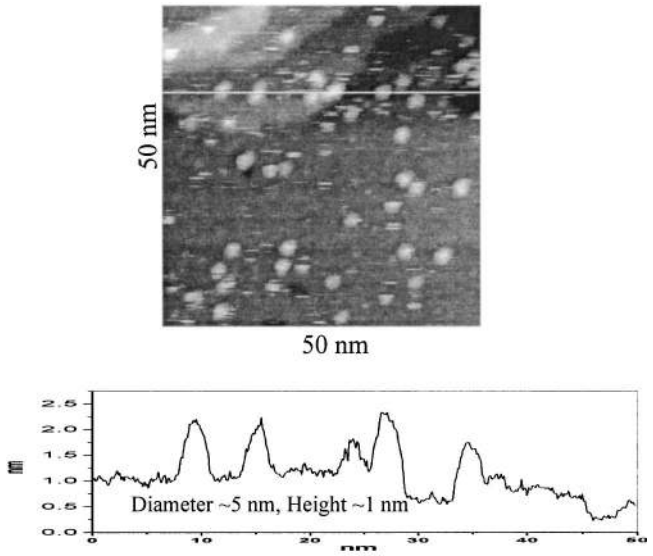

FIG. 8. A 50×50 nm STM image of C_{60}-functionalized 11-AUT SAM on Au(111) surface. Image taken at 0.08 nA/400 mV at 1.02 Hz / 1.5 nm.

tine C_{60} is also lifted in the SAM as a result of amine addition to C_{60}. The calculations were done for ground-state configuration of the molecules with DFT at level Becke's three-parameter exchange functional combined with the Lee, Yang, and Parr's correlation functional (B3LYP), as implemented in GAUSSIAN 98 (Ref. 55) program package, withstanding the fact that excitonic interactions between the excited electron and the core hole left behind as a result of absorption, give a final state, significantly different from the ground state.

4. STM of the C_{60}-functionalized 11-AUT self-assembled monolayer

Unlike alkane thiol SAMs, the STM image of 11-AUT SAM was found to be associated with roughness, anticipated of a hydrophilic surface with $-NH_2$ end group. Metastable coadsorbate formation as a result of end group reaction with solvent and/or air/moisture leading to probable H bonding could have hampered the high resolution of these images.[56] Etch pits of varying size from ~1.8 to 2.8 Å are seen in the section analysis of the image, which is against ~2.5 Å observed for alkane thiol SAMs. A larger number of such pits in cysteamine SAM as compared to propanethiol/alkanethiol SAM were explained to be due to slower migration rate of the adsorbate-Au complex arising from substantial interaction between the $-NH_2$ group and Au and further due to possible hydrogen bonding between the NH_2 groups, leading to a rigid monolayer structure.[57]

Figure 8 shows the STM image of a C_{60}-functionalized 11-AUT monolayer showing a distinct difference from that of 11-AUT SAM. The image demonstrates substantial coverage of surface-confined moieties, but without any molecular order. STM constant current contours of organic monolayers trace a combination of contributions from the Au–S interface and from the monolayer surface. With high gap impedance, the contribution from the monolayer surface is maximized. We thus attribute the bright topographic spots, protruding above the thiol film, to be due to tethered C_{60} molecules which were absent in the STM image of 11-AUT SAM. Further, the stability of the image at low tunneling current implies the C_{60} moieties to be extended above the Au substrate via thiolate tail. In contrary, much larger currents were required for imaging the unfunctionalized C_{60} thin films on metal surfaces.[58–60] We notice the distribution of these on several terraces simultaneously and are almost spherical and of similar size. The diameter of each of such unit, upon section analysis, came out to be ~5 nm, attributing the spots to be 2D C_{60} aggregates, $(C_{60})_n$, where $n\sim5$.

A high resolution image is shown in Fig. 9 depicting the structure of one such aggregate. Controlled layering of 2D *J* aggregates of anionic cyanine dye on self-assembled cysteamine monolayer on Au(111) are reported in conjunction with our observation.[61] The dark features in the figure are due to underlying Au and gray areas are thiol domains. Thiol

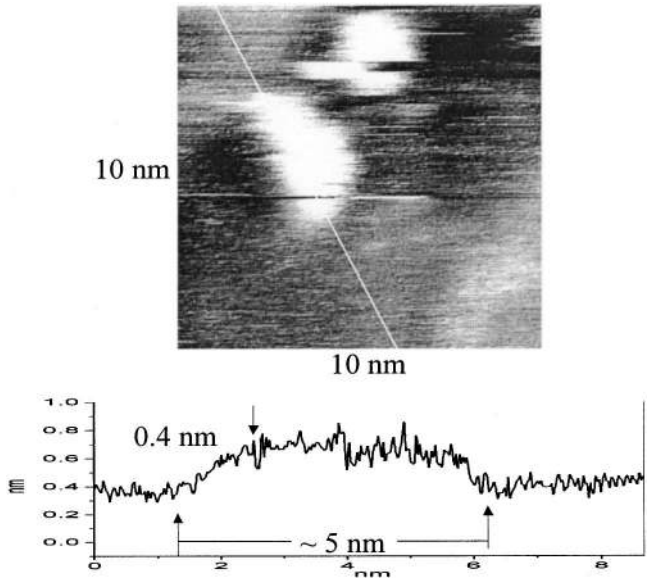

FIG. 9. STM images of 10×10 nm of C_{60}-functionalized 11-AUT SAM on Au(111) surface. Image taken at 0.10 nA/500 mV at 5.79 Hz/0.6 nm.

films have demonstrated domains of $(\sqrt{3}\times\sqrt{3})R30°$ and related structures resulting from different alkyl chain tilt vectors and sulphur head group registry.[62] However, we do not observe them. Presumably, the C_{60} moieties are inserted at the grain boundaries in the thiol lattice and the asymmetric shape of the protrusions probably arises from the tip effect.[63] The prominent height difference in the figure can be interpreted to arise as a function of local density of states as well as the local barrier height.[64]

5. The origin of C_{60} Aggregation

With a similar magnitude of the specific surface energies of interaction among the C_{60} and the solvent molecules, the fullerene molecules in solution undergo cluster formation. The latter is correlated with the extraordinary physical and chemical peculiarities of C_{60} in solution with respect to thermodynamic, kinetic, and optical properties. The process of aggregation can be conceived to be a phase transition of the system that has analogous counterparts in colloidal solutions, where the most commonly observed phase transition is solidification with formation of a condensed phase with a regular crystal structure.[65] Further, this phase behavior at ~1-mM concentration can be entropically driven by steric repulsion between the particles, complying with the fact that they are negatively charged.[24] Entropy maximization occurs by minimizing free-energy $G=U-TS$ with U, the internal energy =0 for hard and impenetrable particles.[66] Once formed, the aggregates are bound to each other with a certain magnitude of cohesive energy.[67] The isolated C_{60} molecule was calculated to have a cohesive energy of 7.4 eV/at., whereas the calculated cohesive energy (from total-energy calculations) per C_{60} molecule in a fcc lattice was estimated to be 1.6 eV, which is, however, much smaller than the typical C–C bond energy of ~3 eV. Introduction of an organized monolayer assembly of 11-AUT on Au(111) into a millimolar solution of C_{60} in benzene, comprising of monomeric and aggregated C_{60} clusters, could thus result in $-NH_2$ bonding to the monomeric/aggregated C_{60} moieties existing in the solution. However, the C_{60} bonding and aggregation would depend strongly on the density of the surface amino groups, and aggregation can take place only at positions where the C_{60} molecules are already available. The overall stability in energy of this unique surface phase will depend on the cohesive interaction between individual C_{60} molecules in the resultant aggregate and C_{60}'s interaction with the surface amino groups.

Using the above experimental results based on NEXAFS spectroscopy and STM, we propose a probable domain growth mechanism for the C_{60}-functionalized 11-amino-1-undecane thiol self-assembly on Au(111) surface. According to this, aminothiol molecules preferentially nucleate/physisorb along the boundaries of existing and oriented thiolate domains with a molecular tilt angle of ~56°. This forms at an early stage of film formation obeying adsorption-limited mass transfer from bulk to the substrate. A high reaction probability for C_{60} along the perimeters of a thiolate domain thus could lead to its interaction with the chemisorbed as well as the physisorbed amino thiolate/thiol species, upon exposing the 11-AUT SAM on Au(111) to a millimolar solution of C_{60} in benzene. More specifically, the C_{60} solution with its monomeric component will interact with the oriented islands that can act as templates with substantial van der Waals interaction between the $-CH_2$ chains (~2 kJ/mol per $-CH_2$ group in a van der Waals alkane crystal).[68] Complying with the above is the similar magnitude of tilt angle, ~56°–57°, obtained for both the SAM systems. The bonded C_{60} further aggregates, wherein an individual molecule in the resultant aggregate is subject to cohesive interaction between them, keeping intact its interaction with the surface amino groups. On the other hand, $(C_{60})_n$ moieties may have an affinity for the unbound thiol islands.

IV. CONCLUSION

The molecular orientation and the molecule-substrate surface structure of self-assembled monolayers of C_{60}-functionalized 11-amino-1-undecane thiol on Au(111) have been investigated by near-edge x-ray-absorption fine structure spectroscopy and scanning tunneling microscopy. While the peak width enhancement of LUMO and reduction in the intensity and peak broadening of the LUMO+1 feature confirmed the asymmetric bonding of surface-anchored $-NH_2$ group of the amino thiol monolayer with C_{60}, the appearance of a new feature in the NEXAFS spectrum confirmed the existence of aggregated C_{60} clusters, further supported from scanning tunneling microscopy. Based on these observations, a domain growth mechanism is proposed where possible existence of separate phases with different orientations and two-dimensional ordering is envisaged. The monolayer assembly growth mechanism at saturation coverage, complying with the reported observations, could be described as a multistep process with several rate constants.

ACKNOWLEDGMENT

Japan Society for Promotion of Sciences (JSPS) is gratefully acknowledged for granting the invitation fellowship to one of the authors (A.P.).

[1] B. Waestberg, S. Lunell, C. Enkvist, P. A. Bruehwiler, A. J. Maxwell, and N. Martensson, Phys. Rev. B **50**, 13031 (1994).
[2] P. A. Heiney, J. Phys. Chem. Solids **53**, 1333 (1992).
[3] S. Satpathy, V. P. Antropov, O. K. Andersen, O. Jepsen, O. Gunnarsson, and A. I. Leichtenstein, Phys. Rev. B **46**, 1773 (1992).
[4] J. H. Weaver, J. L. Martins, T. Komeda *et al.*, Phys. Rev. Lett. **66**, 1741 (1991).
[5] P. A. Bruewiler, A. J. Maxwell, A. Nilsson, R. L. Whetten, and N. Martensson, Chem. Phys. Lett. **193**, 311 (1992).
[6] S. Hasegawa, T. Miyamae, K. Yakushi, H. Inokuchi, K. Seki, and N. Ueno, Phys. Rev. B **58**, 4927 (1998).
[7] M. B. Jost, N. Troullier, D. M. Poisier, J. L. Martins, J. H. Weaver, L. P. F. Chibante, and R. E. Smalley Phys. Rev. B **44**, 1966 (1991).
[8] C. T. Chen, L. H. Tjeng, P. Rudolf *et al.*, Nature (London) **352**, 603 (1991).
[9] L. J. Terminello, D. K. Shuh, F. J. Himpsel, D. A. Lapiano-Smith, J. Stoehr, D. S. Bethune, and G. Meijer, Chem. Phys. Lett. **182**, 491 (1991).
[10] S. Krummacher, M. Biermann, M. Neeb, A. Liebsch, and W. Eberhardt, Phys. Rev. B **48**, 8424 (1993).
[11] A. J. Maxwell, P. A. Bruehwiler, A. Nilsson, and N. Martensson, Phys. Rev. B **49**, 10717 (1994).
[12] P. A. Bruehwiler, P. A. Maxwell, J. Rudolf, C. D. Gutleben, B. Waestberg, and N. Martensson, Phys. Rev. Lett. **71**, 3721 (1993).
[13] X. Shi, W. B. Caldwell, K. C. Chen, and A. Mirkin, J. Am. Chem. Soc. **116**, 11598 (1994).

[14]L. M. Lander, W. J. Brittain, and E. A. Volger, Langmuir **11**, 375 (1995).
[15]K. Chen, W. B. Caldwell, and C. A. Mirkin, J. Am. Chem. Soc. **115**, 1193 (1993).
[16]V. V. Tsukruk, L. M. Lander, and W. J. Brittain, Langmuir **10**, 996 (1994).
[17]C. Yan, A. Goelzhaeuser, and M. Grunze, Langmuir **15**, 2414 (1999).
[18]G. Haener, Ch. Woell, M. Buck, and M. Grunze, Langmuir **9**, 1955 (1993).
[19]C. Yan, M. Zharnikov, A. Goelzhaeuser, and M. Grunze, Langmuir **16**, 6208 (2000).
[20]J. Stoer, *NEXAFS Spectroscopy* (Springer, Berlin, 1992).
[21]Q. Ying, J. Marecek, and B. Chu, J. Chem. Phys. **101**, 2665 (1994).
[22]V. N. Bezmel'nitsyn, A. V. Eletskii, and E. V. J. Stepanov, J. Phys. Chem. **98**, 6665 (1994).
[23]Q. Ying, J. Marecek, and B. Chu, Chem. Phys. Lett. **219**, 214 (1994).
[24]A. G. Rossitza, D. Shigeru, and K. Tsujii, J. Am. Chem. Soc. **123**, 10460 (2001).
[25]S. Nath, H. Pal, D. K. Palit, A. V. Sapre, and J. P. Mittal, J. Phys. Chem. B **102**, 10158 (1998).
[26]V. N. Bezmel'nitsyn, A. V. Eletskii, and E. V. J. Stepanov, in *Progress in Fullerene Research*, edited by H. Kuzmany (World Scientific, Singapore, 1994), p. 45.
[27]A. E. Hooper, D. Werho, T. Hopson, and O. Palmer, Surf. Interface Anal. **31**, 809 (2001).
[28]D. Kondo, K. Sakamoto, H. Takeda, and F. Matsui, K. Amemiya, T. Ohta, W. Uchida, and A. Kasuya, Surf. Sci. **514**, 337 (2002).
[29]M. Himmelhaus, I. Gauss, M. Buck, F. Eisert, Ch. Woell, and M. Grunze, J. Electron Spectrosc. Relat. Phenom. **92**, 139 (1998).
[30]C. Yan, M. Zharnikov, A. Goelzhauser, and M. Grunze, Langmuir **16**, 6208 (2000).
[31]C. Yan, A. Goelzhauser, and M. Grunze, Langmuir **15**, 2414 (1999).
[32]G. Hahener, Ch. Woell, M. Buck, and M. Grunze, Langmuir **9**, 1955 (1993).
[33]J. Hasselstroem, O. Karis, M. Weinelt *et al.*, Surf. Sci. **407**, 221 (1998).
[34]I. H. Campbell, S. Rubin, T. A. Zawodzinzki, J. D. Kress, R. L. Martin, and D. L. Smith, Phys. Rev. B **54**, R14321 (1996).
[35]A. Patnaik, H. Setoyama, and N. Ueno, J. Chem. Phys. **120**, 6214 (2004).
[36]M. Kawasaki, T. Sato, and T. Yoshimoto, Langmuir **16**, 5409 (2000).
[37]L. A. Bumm, J. J. Arnold, M. J. Cygan *et al.*, Science **271**, 1705 (1996).
[38]K. F. Kelly, Y. S. Schon, T. R. Lee, and N. J. Halas, J. Phys. Chem. **103**, 8639 (1999).
[39]A. Bokare and A. Patnaik, J. Phys. Chem. B **107**, 6079 (2003).
[40]M. Takata *et al.*, presented at the Autumn Meeting (46th Nenkai) of the Physical Society of Japan, University of Hokkaido, 1991 (unpublished).
[41]Y. Saito, N. Suzuki, H. Shinohara, and Y. Ando, Jpn. J. Appl. Phys., Part 1 **30**, 2857 (1991).
[42]M. F. Meidine, P. B. Hitchcock, H. W. Kroto, R. Taylor, and D. R. M. Walton, J. Chem. Soc., Chem. Commun. **20**, 1534 (1992).
[43]D. L. Corset, J. Phys. Chem. B **99**, 16748 (1995).
[44]D. A. Outka and J. Stoehr, in *Chemistry and Physics of Solid Surfaces VII*, Springer Series in Surface Sciences Vol. 10, edited by V. R. Vanselow and R. Howe (Springer, Berlin, 1998), p. 201.
[45]D. L. Lichtenberger, K. W. Nebesny, C. D. Ray, D. R. Hoffman, and L. D. Lamb, Chem. Phys. Lett. **176**, 203 (1991).
[46]C. T. Tzeng, W.-S. Lo, J.-Y. Yuh, R.-Y. Chu, and K.-D. Tsuei, Phys. Rev. B **61**, 2263 (2000).
[47]K. Sakamoto, D. Kondo, H. Takeda *et al.*, Surf. Sci. **493**, 604 (2001).
[48]K.-D. Tsuei, J. Y. Yuh, C. T. Tzeng, R.-Y. Chu, S.-C. Chung, and K.-L. Tsang, Phys. Rev. B **56**, 15412 (1997).
[49]A. J. Maxwell, P. A. Bruehwiler, D. Arvanitis, J. Hasselstroem, M. K.-J. Johansson, and N. Martensson, Phys. Rev. B **57**, 7312 (1998).
[50]R. Mitsumoto, J. Phys. Chem. **102**, 552 (1998).
[51]S. Saito and A. Oshiyama, Phys. Rev. Lett. **66**, 2637 (1991).
[52]F. Diederich, J. Effing, U. Jonas, L. Jullien, T. Plesnivy, H. Ringsdorf, C. Thilgen, and D. Weinstein, Angew. Chem., Int. Ed. Engl. **31**, 1599 (1992).
[53]P. A. Bruehwiler, A. J. Maxwell, and N. Martensson, Int. J. Mod. Phys. B **6**, 3923 (1992).
[54]M. B. Jost, N. Troullier, D. M. Poirier, J. L. Martins, J. H. Weaver, L. P. F. Chibante, and R. E. Smalley, Phys. Rev. B **44**, 1966 (1991).
[55]M. J. Frisch, G. W. Trucks, H. B. Schlegel *et al.*, GAUSSIAN, Gaussian Inc., Pittsburg, PA, 1998.
[56]E. Delamarche and B. Michel, Thin Solid Films **273**, 54 (1994).
[57]S. Y. Lee, J. Noh, E. Ito, M. Hara, and H. Lee, Jpn. J. Appl. Phys., Part 1 **42**, 1 (2003).
[58]Y. S. Shon, K. F. Kelly, N. J. Halas, and T. R. Lee, Langmuir **15**, 5329 (1999).
[59]R. J. Wilson, G. Meijer, D. S. Bethune, R. D. Johnson, D. D. Chambliss, M. S. deVries, H. E. Hunziker, and H. R. Wendt, Nature (London) **348**, 621 (1990).
[60]T. Hashizume, K. Motai, X. D. Wang *et al.*, Phys. Rev. Lett. **71**, 2959 (1993).
[61]M. Kawasaki, T. Sato, and T. Yoshimoto, Langmuir **16**, 5409 (2000).
[62]L. A. Bumm, J. J. Arnold, M. T. Cygan, *et al.* Science **271**, 1705 (1996).
[63]K. F. Kelly, Y. S. Schon, T. R. Lee, and N. J. Halas, J. Phys. Chem. **103**, 8639 (1999).
[64]N. D. Lang, Phys. Rev. Lett. **58**, 45 (1987).
[65]N. Asherie, A. Lomakin, and G. B. Benedek, Phys. Rev. Lett. **77**, 4832 (1996).
[66]P. A. Forsyth, S. Marcedja, Jr., D. J. Mitchell, and B. W. Ninham, Adv. Colloid Interface Sci. **9**, 37 (1978).
[67]S. Saito and A. Oshiyama, Phys. Rev. Lett. **66**, 2637 (1991).
[68]A. Perstin and M. Grunze, Langmuir **10**, 3668 (1994).